

# Atmospheric turbulences over Guwahati and their association with tropospheric dynamics

A Medhi<sup>§,\*</sup>, M Devi, H Goswami & A K Barbara

Department of Physics, Gauhati University, Guwahati 781 014, Assam, India

<sup>§</sup>E-mail: alaka.medhi05@gmail.com

*Received 6 August 2014; revised 4 March 2015; accepted 9 March 2015*

The paper presents an analysis of structure constant parameter ( $Cn^2$ ) over Guwahati (26.2°N, 91.75°E) in relation to tropospheric dynamics involving atmospheric variabilities, like temperature, potential temperature and specific humidity. Data collected from radiosonde operated at Guwahati are utilised for drawing seasonal profiles of  $Cn^2$  up to the tropopause height. The results show that depending on season, the average values of  $Cn^2$  may vary between  $10^{-14.5}$  and  $10^{-19} \text{ m}^{-2/3}$  and that their magnitude decreases gradually to reach a minimum of  $-18.3 \text{ m}^{-2/3}$  at around 10 km and then starts increasing up to the tropopause height of 15-16 km. The analysis, further, demonstrates that  $Cn^2$  value reaches maximum in summer and minimum in winter, within the height range of 1-10 km. But beyond the altitude of 10 km,  $Cn^2$  shows higher values in winter as compared to its summer time counterparts. The paper also highlights that at pre earthquake (EQ) ambiances, this parameter may dip down by two to three orders of magnitude from its average normal range. The seasonal transition pattern of  $Cn^2$  with height and the EQ time changes in  $Cn^2$  features are put to a correlative analysis with the tropospheric dynamics for an explanation.

**Keywords:** Atmospheric structure constant, Tropospheric temperature, Potential temperature gradient, Specific humidity, Atmospheric turbulence

**PACS Nos:** 92.60.hk; 92.60.hf

## 1 Introduction

The atmospheric structure constant ( $Cn^2$ ), is a parameter that reflects random fluctuations of atmospheric refractive index. In steady conditions, this index decreases monotonically with height, but the atmospheric medium often remains in a turbulent state caused by factors such as irregular heating of the earth's surface, forced cooling and also by natural or manmade perturbations. These turbulent states, generally, produce eddies with spatial and temporal scales. Such eddies carry turbulent kinetic energy (TKE), i.e. the energy per unit mass associated with eddies. In the process of dissipations in the atmospheric medium, large eddies shrink to small eddies, resulting in decrease of TKE to zero, a process known as inertial cascade process. Such transfer of large eddies to small one transferring their energy into the medium, is generally proportional to the dissipation rate. Therefore, atmospheric cascade process is associated with transfer of energy from the kinetic field leading to formation of irregularities and eddies in the fluid<sup>1</sup>. The size of the irregularities is defined by the parameter  $Cn^2$ .

During recent years, there has been emphasis on understanding the lower atmospheric dynamics through analysis of  $Cn^2$  features in diurnal and

seasonal terms<sup>2-6</sup>. This parameter is also used for predicting fast changing fluctuation and attenuation of radio waves while travelling through lower atmosphere<sup>7-9</sup>. Further, as lower atmospheric dynamics are highly sensitive to variations in temperature, pressure and humidity,  $Cn^2$  may suffer changes with atmospheric situation, like in worst weather ambiances<sup>3,10</sup>. One can, therefore, expect modification of this parameter by earthquake (EQ) preparatory processes when atmospheric variabilities get modulated by seismic induced energy sources<sup>11,12</sup>.

With the above background, the paper aims at to characterize the seasonal variation of  $Cn^2$  over Guwahati (26.2°N, 91.75°E) using five years of Radiosonde (RS) data available from Regional Meteorological Centre, Guwahati and Wyoming University. Further, the paper examines possible role of EQ induced effects, if any, on  $Cn^2$ , during a few major EQ events.

## 2 Data and Methodology

In this paper,  $Cn^2$  is determined by using RS data. The RS contains a radio transmitter with sensors to measure pressure, temperature, humidity as well as wind speed and direction at different heights of the

atmosphere starting from the surface to around 30 km. The entire package of transmitter and sensors is carried aloft by a spherically shaped free flying balloon released from surface, generally, two times a day, i.e. at 0000 and 1200 hrs UTC. The data launched at different meteorological stations around the world are available to public users, provided by the University of Wyoming (<http://weather.uwyo.edu/upperair/sounding.html>). The  $Cn^2$  values are calculated by using Eqs (1) and (2) with the data from the above website.

The expression for  $Cn^2$  is defined by Eq. (1) as<sup>7</sup>:

$$Cn^2 \equiv a^2 \infty' l_0^{\frac{4}{3}} M^2 \quad \dots (1)$$

where,  $a^2$ , is a dimensionless constant within 1.5 and 3.5 but most commonly taken as 2.8 (Ref. 13);  $\infty'$ , a numerical constant, generally, taken as unity;  $l_0$ , the buoyancy/outer scale length of the turbulence spectrum; and  $M$ , the vertical gradient of potential refractive index fluctuations. This gradient is expressed as<sup>14,15</sup>:

$$M = -77.6 \times 10^{-6} \left( \frac{P}{T} \right) \left( \frac{\partial \ln \theta_T}{\partial Z} \right) \left[ 1 + \frac{15500}{T} \left( 1 - \frac{1}{2} \frac{\partial \ln q / \partial Z}{\partial \ln \theta_T / \partial Z} \right) \right] \quad \dots (2)$$

where,  $T$ , is the ambient temperature in K;  $P$ , the pressure;  $q$ , the specific humidity (SH); and  $\theta_T$ , the potential temperature (PT), given as:

$$\theta_T = T \times \left( \frac{P_0}{P} \right)^{0.3} \quad \dots (3)$$

where,  $P_0$ , is the standard atmospheric pressure; and  $Z$ , the height in meters.

The total turbulent energy density spectrum consists of a production region, the inertial sub-range and the dissipation region. Most of the turbulence production energy input occurs at scale sizes between  $6l_0$  and  $l_0/6$ , where,  $l_0/6$ , is defined as the onset of the inertial sub-range. The outer scale  $l_0$  is presumed to be around  $10 \text{ m}^{10}$ , although no direct evidence is available on the thickness of a turbulent layer<sup>3</sup>.

Taking RS data at an interval of 1 km height, the gradients of potential temperature ( $\partial\theta/\partial z$ ) and specific humidity ( $\partial q/\partial z$ ) are computed up to the height of 15 km. From the gradients so obtained,  $M$  values are calculated by using Eq. (2) and  $Cn^2$  profile is then

drawn [Eq. (1)] for morning and evening hours of each day taking  $l_0$  to be 10 m with values of constants 'a' &  $\infty'$  as 2.8 and 1, respectively<sup>3,4,13</sup>. From these profiles, monthly average  $Cn^2$  value is calculated. Finally, to attain the climatological variation of this parameter, the 5-years mean of monthly average  $Cn^2$  profiles are averaged. In this analysis, June-August are taken as summer months, September-November as autumnal equinox and December-February as winter season while months from March-May cover vernal equinox period.

### 3 Results and Discussion

Considering the significant role played by PT and SH on  $Cn^2$  [Eq (2)], it is essential to analyse variation pattern of these two parameters with height. Therefore, PT and SH from 1 to 15 km altitude are calculated using temperature, humidity and pressure data of RS for each day of a month. In Figs 1(a and b), summer time representative profiles for PT and SH, respectively are presented. The figure shows that PT decreases with a constant rate up to the height of 9-10 km but beyond this altitude, a break in the PT gradient is noted. The SH profile also presents a constant decrease of its value up to a height of 6 km but its gradient changes once it crosses this altitude and attains zero value at a height of 10 km. Next, from the SH and PT profiles, the value of  $M$  is calculated using Eq. (2) individually for each day from the total of 3000 such profiles covering five-year study period. Finally, Eq. (1) is used for evaluating  $Cn^2$  profile from 1 to 15 km height by incorporating the corresponding vertical gradient of potential refractive index value ( $M$ ). The profiles of  $M$  and  $Cn^2$  for each month is drawn by averaging each day profile of a month and the 3-months mean is then calculated to receive the seasonal pattern. The height variation of  $M$  and  $\log Cn^2$  of a summer day of the year 2007 are presented in Figs 1(c and d), as a representative profile of this month. The breakdown in the slope of  $M$  profile at a height of 8-10 km [Fig. 1(c)] is similar to that observed in the PT variation pattern of Fig. 1(a). It is seen that  $\log Cn^2$  varies from  $-14 \text{ m}^{-2/3}$  to  $-18.8 \text{ m}^{-2/3}$  up to the height of 10 km but above this altitude, it shows an abrupt increase till it reaches the tropopause height. In general,  $Cn^2$  attains the highest value within the height interval of 1-3 km. In the middle troposphere (3-10 km), the  $\log Cn^2$  value gradually decreases to reach minimum ( $-18.8 \text{ m}^{-2/3}$ ) at a height of 9-11 km.

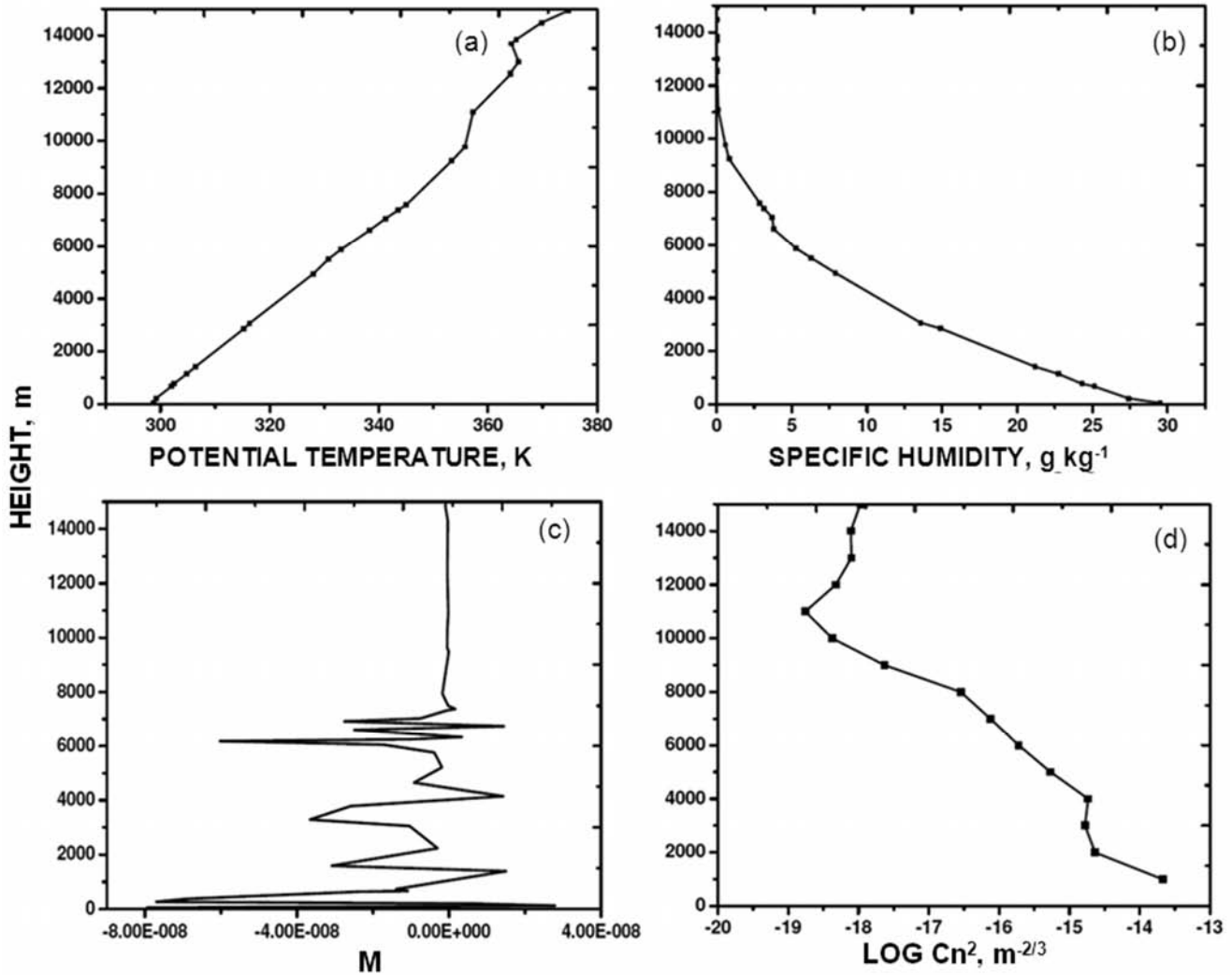


Fig. 1 — Profiles of: (a) Potential temperature (PT); (b) Specific humidity (SH); (c) Potential refractive index gradient; and (d) Refractive index structure constant parameter ( $Cn^2$ ) (representative pattern)

**3.1 Month-to-month variation of  $Cn^2$**

From large number of individual profiles, variation of  $Cn^2$  for each month is calculated. The  $\log Cn^2$  - height profile so obtained is then averaged for each month covering five-year period and the profiles so obtained are presented in Fig. 2.

The finer features of  $\log Cn^2$  for each month within the height range 1-15 km are presented in Table 1. It is seen from the table that over Guwahati,  $\log Cn^2$  may reach a maximum value of  $-14.3 \text{ m}^{-2/3}$  and a minimum of  $-18.3 \text{ m}^{-2/3}$ , which varies from month-to-month. Further, the table shows that  $\log Cn^2$  gradually decreases with height up to 10 km in each month and then it changes its value once its crosses this altitude.

Such changes in  $\log Cn^2$  gradient in the range 1-10 km and 10-15 km are shown in Figs 3 (a and b),

respectively. The figure shows that  $Cn^2$  attains maximum value in the months of June and July up to the height of 10 km but beyond this range,  $Cn^2$  abruptly decreases to reach a lowest value as compared to other months of the year.

**3.2 Seasonal variation of  $Cn^2$**

The seasonal  $Cn^2$  profiles are then drawn and five years average seasonal  $\log Cn^2$  - height variation pattern for four seasons is presented in Fig. 4. The profiles show that up to the height of 10 km,  $Cn^2$  attains higher value during summer and autumnal equinox and lowest value during winter and vernal equinox season, but above this altitude  $Cn^2$  goes minimum in summer and maximum in winter and vernal equinox season as reflected in profiles of each individual month of Fig. 2.

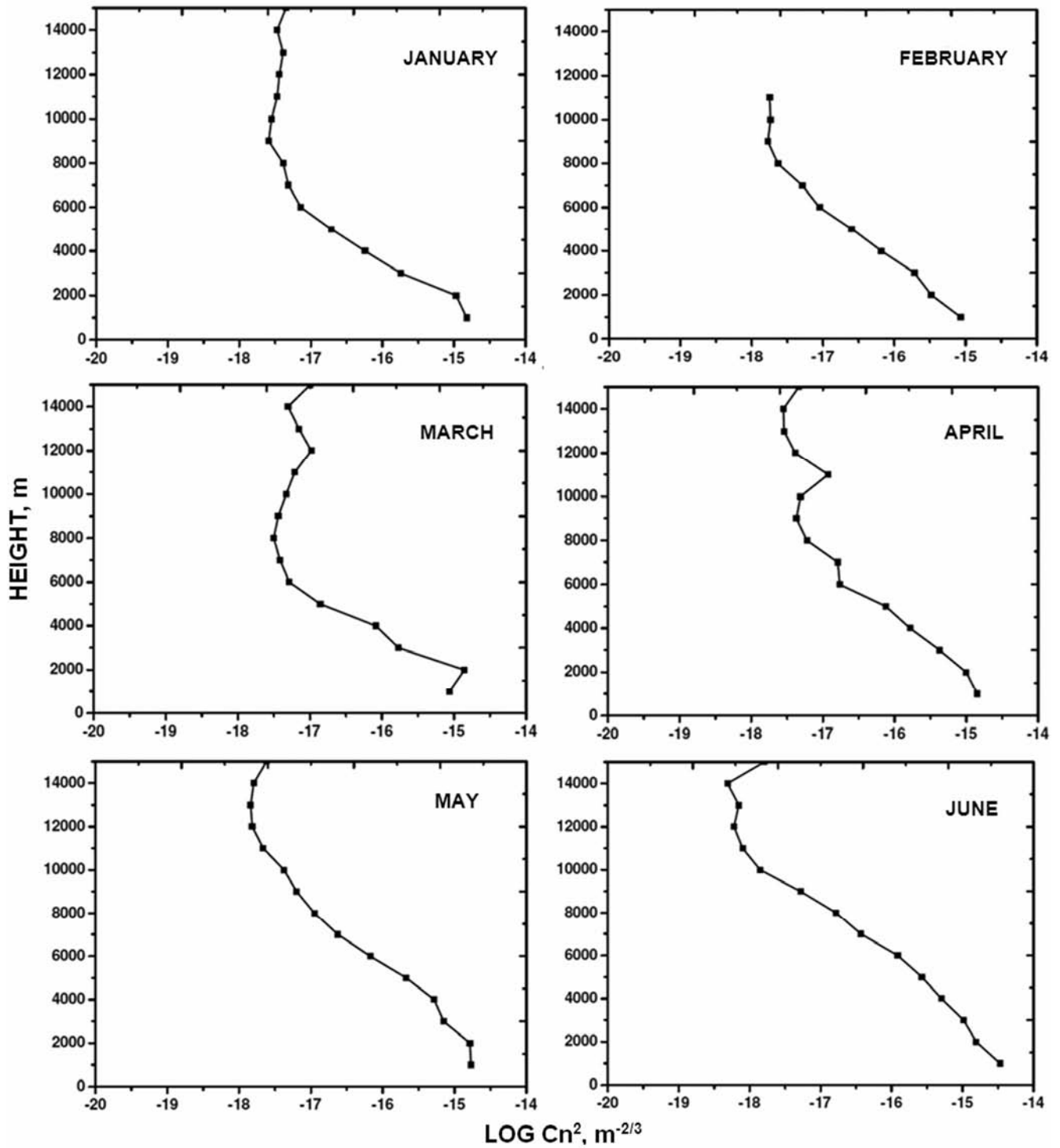


Fig. 2 — Climatological (2006–2010) mean of  $\log Cn^2$  for different months (January–December) over Guwahati (Contd.)

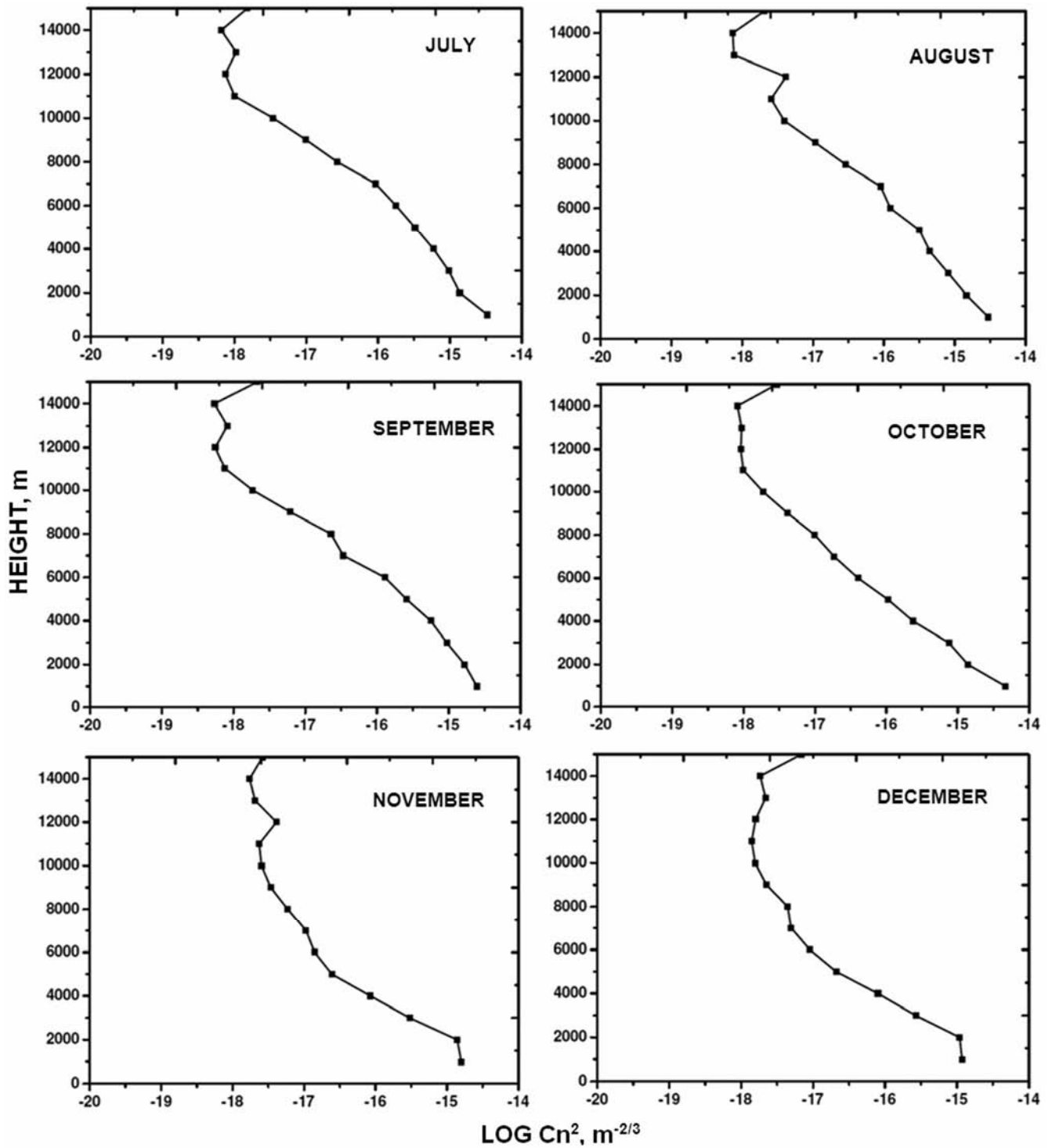
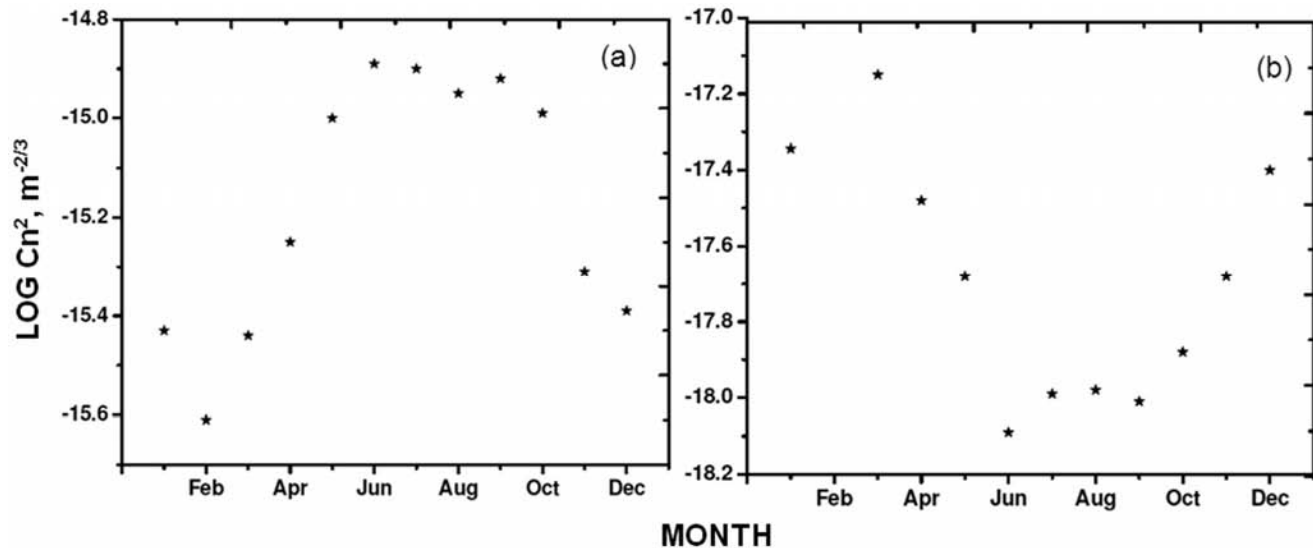


Fig. 2 (Contd.) — Climatological (2006–2010) mean of  $\log Cn^2$  for different months (January–December) over Guwahati

Table 1 — Mean of  $\log Cn^2$  for different months (January–December) over Guwahati during 2006-2010

Height, m	January	February	March	April	May	June	July	August	September	October	November	December
1000	-14.84	-15.07	-15.07	-14.85	-14.77	-14.47	-14.48	-14.52	-14.61	-14.33	-14.80	-14.93
2000	-15.08	-15.48	-14.86	-15.00	-14.78	-14.81	-14.86	-14.83	-14.78	-14.86	-14.86	-14.96
3000	-15.62	-15.72	-15.77	-15.37	-15.15	-14.98	-15.02	-15.09	-15.03	-15.12	-15.52	-15.57
4000	-16.17	-16.18	-16.08	-15.79	-15.28	-15.30	-15.23	-15.35	-15.25	-15.63	-16.07	-16.10
5000	-16.64	-16.59	-16.86	-16.12	-15.67	-15.57	-15.48	-15.50	-15.59	-15.98	-16.61	-16.68
6000	-17.08	-17.05	-17.29	-16.77	-16.17	-15.91	-15.75	-15.91	-15.89	-16.40	-16.85	-17.04
7000	-17.29	-17.29	-17.41	-16.79	-16.62	-16.43	-16.03	-16.05	-16.47	-16.73	-16.97	-17.31
8000	-17.28	-17.63	-17.50	-17.22	-16.95	-16.78	-16.57	-16.54	-16.64	-17.00	-17.23	-17.35
9000	-17.47	-17.77	-17.44	-17.37	-17.20	-17.28	-17.00	-16.97	-17.21	-17.38	-17.47	-17.65
10000	-17.35	-17.73	-17.33	-17.31	-17.37	-17.85	-17.46	-17.41	-17.73	-17.73	-17.59	-17.80
11000	-17.31	-17.75	-17.21	-16.93	-17.66	-18.10	-17.99	-17.59	-18.12	-18.00	-17.63	-17.85
12000	-17.17		-16.98	-17.39	-17.82	-18.22	-18.13	-17.38	-18.26	-18.04	-17.39	-17.80
13000	-17.33		-17.15	-17.54	-17.84	-18.15	-17.97	-18.12	-18.09	-18.03	-17.68	-17.66
14000	-17.42		-17.30	-17.55	-17.59	-18.31	-18.18	-18.13	-18.26	-18.09	-17.76	-17.38
15000	-17.28		-16.99	-17.34	-17.62	-17.79	-17.82	-17.69	-17.67	-17.54	-17.58	-17.16

Fig. 3 —  $\log Cn^2$  variation at: (a) lower and (b) higher heights

### 3.3 Relation of $Cn^2$ with Earthquake (EQ)

The key parameters in modifying irregularity size is temperature and humidity, therefore, whenever there is a significant change in these parameter, its effect on  $Cn^2$  is also observed. One such situation is the EQ preparatory process. Because there are large number of reports on changes in temperature before and during an EQ, be it surface temperature, the sea surface temperature (SST) or surface latent heat flux (SLHF)<sup>12,16-24</sup>. It is expected to see the effect in the turbulence size structure at EQ time. Therefore,  $Cn^2$  gradient is examined before a few strong EQs events (Table 2).

#### 3.3.1 China earthquake on 12 May 2008

The China EQ of magnitude 7.9 occurred at 31.021°N and 103.367°E on 12 May 2008. On this occasion, surface  $Cn^2$  value for each day of the EQ month May 2008 is calculated and the profile so obtained is presented in Fig. 5. One can see that there is a drastic reduction in  $Cn^2$  by 12.5% from its average just one day prior to the EQ day. Along with the  $Cn^2$  variation for May 2008, the day-to-day variation of  $Cn^2$  is presented in Fig. 5 for May 2009 where there was no EQ, i.e. there was no major EQ ( $M > 7$ ) over this region. The abnormal decrease of  $\log Cn^2$  reaching a value as low as  $-18 \text{ m}^{-2/3}$  on 11 May 2008 suggests

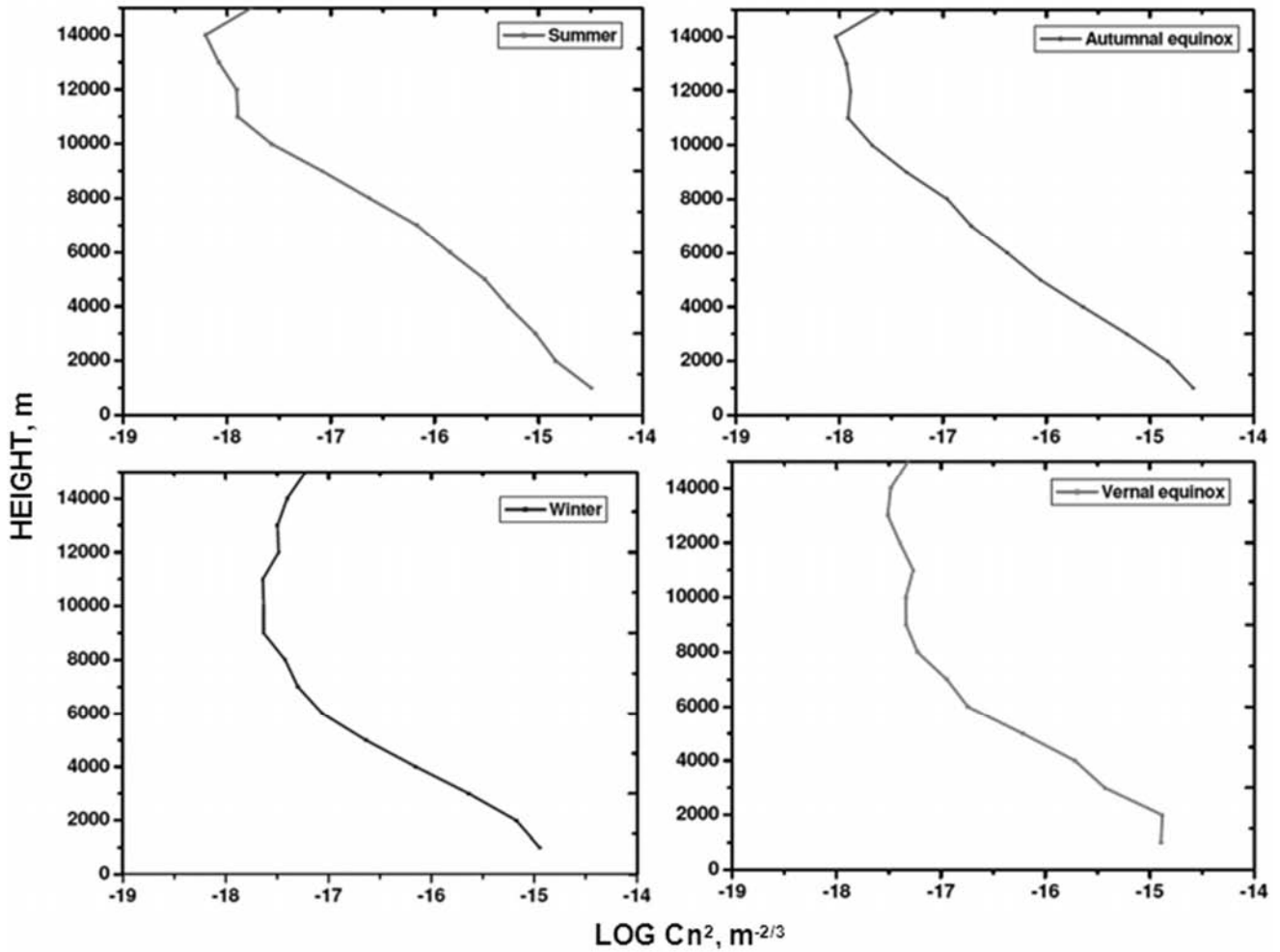


Fig. 4 — Seasonal variation of  $\log Cn^2$  for the summer, autumnal equinox, winter and vernal equinox

Table 2 — Earthquakes under consideration					
S No	Date	Epicenter position		Depth, km	Magnitude
		Latitude, °N	Longitude, °E		
1	12.05.2008	31.021	103.367	33	7.9
2	11.0.2011	38.322	142.369	30	9
3	09.01.2013	25.4	94	75	5.9

possible contribution of EQ preparatory processes in modifying the structure constant parameter.

### 3.3.3 Japan earthquake on 11 March 2011

The Japan EQ of magnitude 9 occurred at 38.322°N and 142.369°E on 11 March 2011. In this event too,  $\log Cn^2$  values near to the epicentre, as presented in Fig. 6, display a 13% drop from its normal magnitude, two days before the EQ event. Such changes in  $\log Cn^2$  are not detected in any other day of this or other months. As

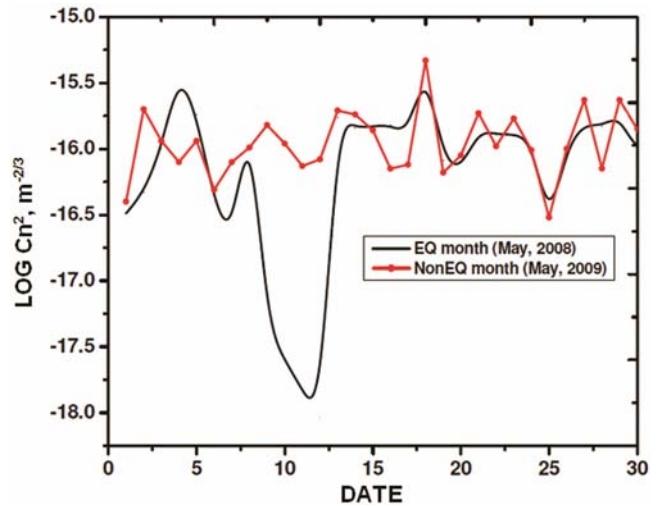


Fig. 5 — Diurnal variation of  $Cn^2$  profile over China for May 2008 [prior, during and after the China earthquake on 12 May 2008 shown by black line and the normal days variation shown by red line]

an example, the  $\log Cn^2$  variation is also presented, for a non-EQ month of March 2010, i.e. there was no major EQ ( $M > 7$ ), in Fig. 6. The figure shows that there was no abnormal variation in this parameter during the non-EQ month and the sudden drop of  $Cn^2$  prior to strong EQ of Japan may be associated with EQ induced effect.

**3.3.3 Myanmar Earthquake on 9 January 2013**

It is also significant to note that even during EQs of moderate strength, there may be situation when marginal changes in  $Cn^2$  may be detected. As an example,  $Cn^2$  variation is presented during a moderate EQ of  $M=5.9$ , that occurred at a location  $25.4^\circ N$  and  $94^\circ E$ , on 9 January 2013. It is seen that  $Cn^2$  at the

epicentre site decreases by 0.4% before the EQ, but unlike the strong EQ events, the change is marginal and recovery period of three days (Fig. 7) from the EQ time  $Cn^2$  to its average value is large.

In order to associate such changes in  $Cn^2$  with the EQ events, the modification in temperature are further calculated. For this purpose the diurnal peak of temperature, i.e.  $T_{max}$  is extracted for each day and the average  $T_{max}$  value is calculated for the EQ month. The percentage deviations in maximum temperature ( $\delta T_{max}$ ) is calculated from their monthly average values and the result is plotted in Fig. 8. It is noted that in all the three EQ cases there is a significant drop in temperature near the epicenter position as marked in Fig. 8. In the China EQ of 12 May 2008,

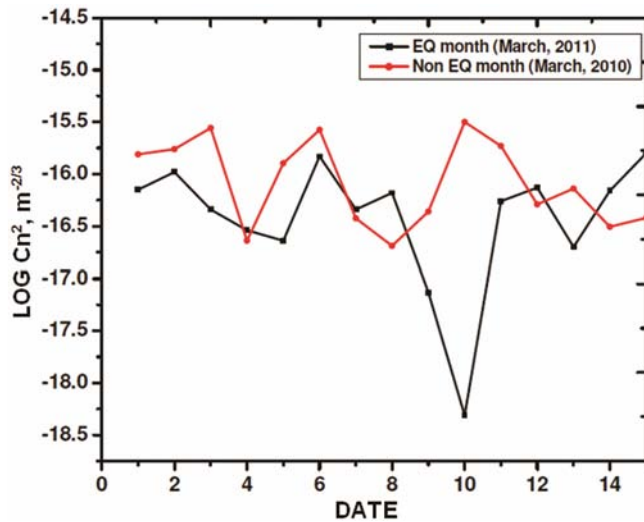


Fig. 6 — Diurnal variation of  $Cn^2$  profile over Japan for March 2011 [prior, during and after the Japan earthquake on 11 March 2011 shown by black line and normal days variation shown by red line]

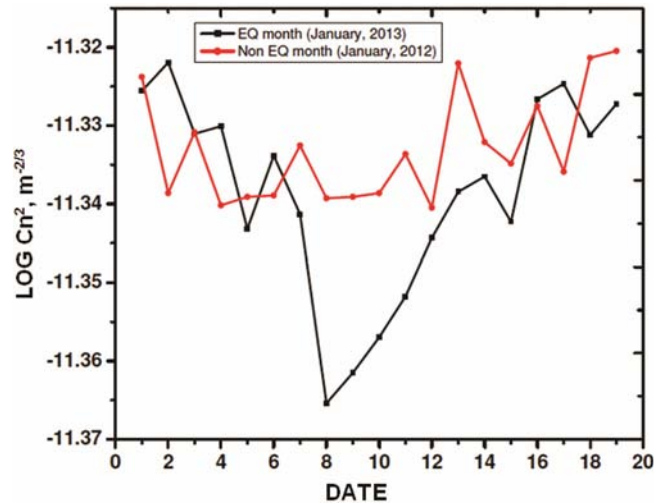


Fig. 7 — Diurnal variation of  $Cn^2$  profile [prior, during and after the earthquake of 9 January 2013 (marked in black);  $Cn^2$  variation during a non-EQ month presented by red line]

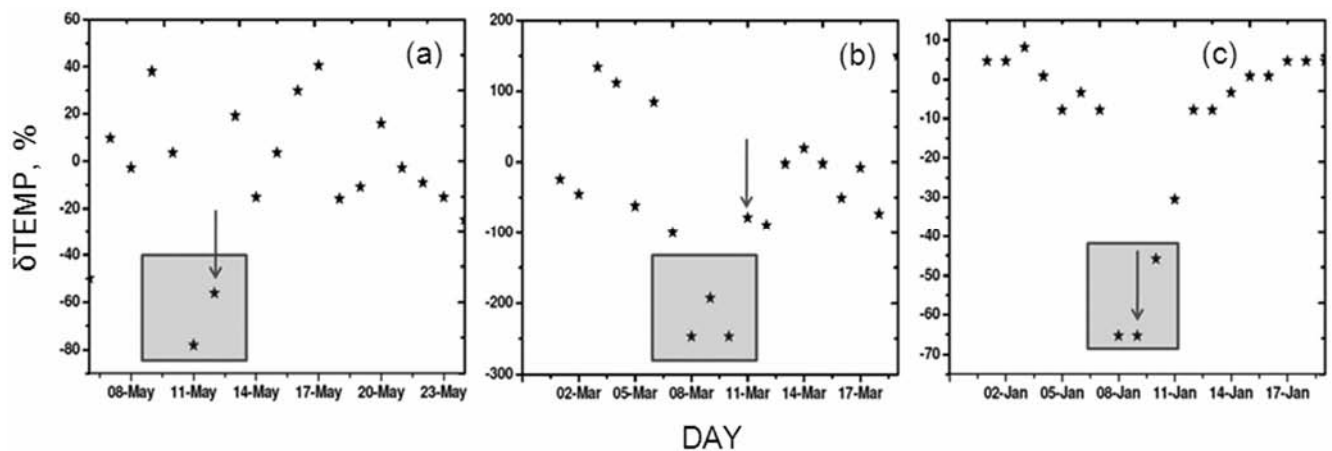


Fig. 8 — Percentage deviations of temperature from the average magnitude for: (a) China; (b) Japan; and (c) Myanmar EQ [arrow shows the EQ day]

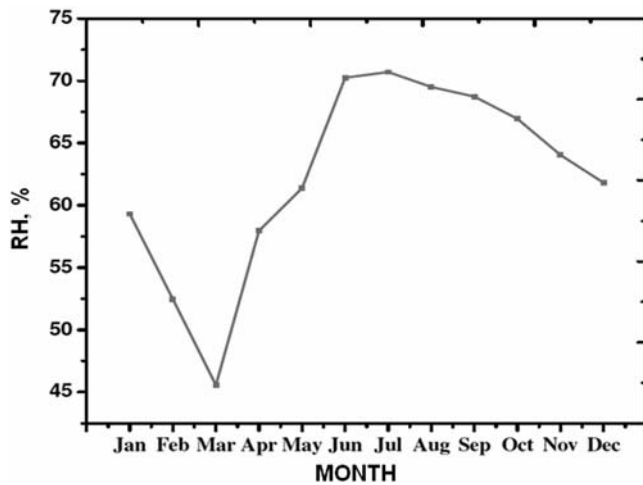


Fig. 9 — Five years (2006-2010) average mean relative humidity variation over Guwahati for each month

the temperature decreased by 78% from its average value, while for Japan EQ of 11 March 2011, temperature showed a very strong dip 250% and for moderate EQ of 9 January 2013, a decrease of only 40% from the average  $T_{\max}$  value was noted. However, more case studies on variation of  $Cn^2$  at different EQ magnitudes and depths are planned to be conducted in future.

#### 4 Conclusion

In the present paper, the monthly as well as seasonal characteristics of turbulence parameter ( $Cn^2$ ) over Guwahati (26.2°N, 91.75°E) are analysed and the role of EQ preparatory processes in modifying this parameter is examined.

From the results, it is observed that  $Cn^2$  has wide fluctuations in summer and autumn season than compared to the winter and vernal equinox months. The summer  $Cn^2$  values from the surface up to the 9-11 km height are larger compared to the other seasons. A region of minimum  $Cn^2$  values is observed at nearly 10 km in all seasons where the potential temperature gradients have a significant change. Due to the excess humidity present in the lower atmosphere, it is likely that  $Cn^2$  shows higher values within 1-6 km height<sup>3,6,10</sup>. This factor also has a control in the variation of  $Cn^2$  in its seasonal pattern. In winter and vernal equinox seasons with very low humidity in the background, the  $Cn^2$  attains the lowest value as compared to the summer and autumn months when humidity attains the seasonal peak over Guwahati as is seen from Fig. 9, where five years average seasonal variation characteristics of humidity

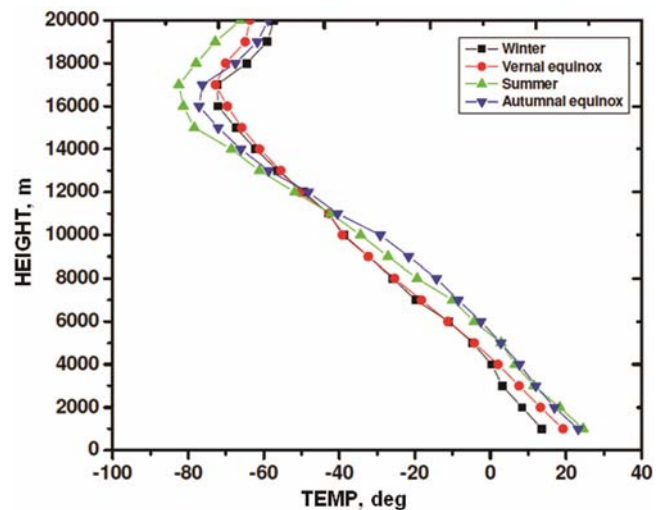


Fig. 10 — Average seasonal variation of temperature with height

(RH) over this station, are shown. The significant low value of RH (40-57%) during winter and vernal equinox months (December–May) and excess of RH (60-70%) in summer and autumn equinox months (June–November) as seen from the figure, might have an effect in controlling the  $Cn^2$  magnitude at different seasons.

Along with humidity, temperature also plays a key role in modifying  $Cn^2$ . In this regard, the temperature profile over Guwahati in different seasons is presented in Fig. 10. It is seen from the figure that temperature maintains the expected pattern up to 10 km height where summer values are higher as compared to winter and vernal equinox season. But it is interesting enough to note a break in the profile at around 10 km height, when temperature during summer shows a decrease in its value as compared to winter and vernal equinox season. This feature is similar to that observed in  $Cn^2$  profile in Fig. 4 indicating a significant role played by temperature and humidity on the structure constant parameter.

#### References

- 1 Justus C G, A theory for the energy spectrum of shear - dependent turbulence, *J Atmos Sci (USA)*, 26 (1969) pp 1238-1244.
- 2 Satheesan K & Krishna Murthy B V, Turbulence parameters in the tropical troposphere and lower stratosphere, *J Geophys Res (USA)*, 107 (2002) pp 2-13.
- 3 Singh N, Joshi R R, Chun H Y, Pant G B, Damle S H & Vashishtha R D, Seasonal, annual and inter-annual features of turbulence parameters over the tropical station Pune (18°32'N, 73°51'E) observed with UHF wind profiler, *Ann Geophys (Germany)*, 26 (2008) pp 3677-3692.
- 4 Belu R R, Comparison of the refractive index structure constant prediction using radiosonde data to in-situ

- thermosonde measurements, *Proc of 9th International Conference on Communications (COMM)*, Jumper G, Ed (Drexel Univ, Philadelphia, USA), 2012 pp 147-150
- 5 Ghosh A K, Siva Kumar V, Kshore Kumar K & Jain A R, VHF radar observation of atmospheric winds, associated shears and  $Cn^2$  at a tropical location: Interdependence and seasonal pattern, *Ann Geophys (Germany)*, 19 (2001) pp 965-973.
  - 6 Nath D, Ratnam M V, Patra A K, Krishna Murthy B V & Rao S V B, Turbulence characteristics over tropical station Gadanki (13.5°N,79.2°E) estimated using high - resolution GPS radiosonde data, *J Geophys Res (USA)*, 115 (2010) doi: 10.1029/2009JD012347.
  - 7 Tatarskii V I, *Effects of the turbulent atmosphere on wave propagation* (Israel Program for Scientific Translations Ltd, Jerusalem), 1971.
  - 8 Grabner M & Kvicera V, Measurement of the structure constant of refractivity at optical wavelengths using a Scintillometer, *Radio Eng (Czech Republic)*, 21 (2012) 455.
  - 9 Ishimaru A, *Wave propagation and scattering in random media*, 1st reissued ed. (IEEE Press, New York), 1997.
  - 10 VanZandt T E, Green J L, Gage K S & Clark W L, Vertical profiles of refractivity turbulence structure constant: Comparison of observations by the Sunset Radar with a new theoretical model, *Radio Sci (USA)*, 13 (1978) pp 819-829.
  - 11 Dolukahnov M, Propagation of tropospheric waves, in *Propagation of radio waves* (Mir, Moscow), 1971.
  - 12 Devi M, Barbara A K, Ruzhin Yu Ya & Depueva A H, Beyond the horizon propagation of VHF signals: Atmospheric features and earthquake beyond the horizon propagation of VHF signals, atmospheric features and earthquake, *Electron J (Russia)*, 39 (2007) pp 1331-1340.
  - 13 Monin A S & Yaglom A M, *Statistical fluid mechanics* (MIT Press, Cambridge, Mass.), 1971.
  - 14 Warnock J M & VanZandt T E, *A statistical model to estimate the refractivity turbulence structure constant  $Cn^2$  in the free atmosphere*, NOAA Tech Memo ERL AL-10 (1985) 176.
  - 15 Doviak R J & Zrnic D S, *Doppler radar and weather observations* (Academic Press, Orlando, FL), 1993, 468.
  - 16 Alvan H V, Azad F H & Omar H B, Chlorophyll concentration and surface temperature changes associated with earthquakes, *Nat Hazards (Netherlands)*, 64 (2012) pp 691-706.
  - 17 Cervone G, Kafatos M, Napoletani D & Singh R P, Wavelet maxima curves of surface latent heat flux associated with two recent major Greek earthquakes, *Nat Hazard Earth Syst Sci (UK)*, 4 (2004) pp 359-374.
  - 18 Dey S & Singh R P, Surface latent heat flux as an earthquake precursor, *Nat Hazard Earth Syst Sci (UK)*, 3 (2003) pp 749-755.
  - 19 Goswami H, Devi M, Rambabu S, Barbara A K & Prakash K, An analysis of the relation between precipitation and earthquake in the Indian region, *Indian J Radio Space Phys*, 43 (2014) pp 41-47.
  - 20 Ouzounov D, Liu D, Kang C, Cervone G, Kafatos M & Taylor P, Outgoing long wave radiation variability from IR satellite data prior to major earthquakes, *Tectonophysics (Netherlands)*, 431 (2007) pp 211-220.
  - 21 Qiang, Z, Thermal infrared anomaly precursor of earthquake, *Pure Appl Geophys (Switzerland)*, 149 (1997) pp 159-170.
  - 22 Singh R P, Cervone G, Singh V P & Kafatos M, Generic precursors to coastal earthquakes: Inferences from Denali fault earthquake, *Tectonophysics (Netherlands)*, 431 (2007) pp 231-240.
  - 23 Tronin A, Atmosphere-Lithosphere coupling, Thermal anomalies on the earth's surface in seismic process, in *Seismo electromagnetics: Lithosphere-atmosphere-ionosphere coupling*, M Hayakawa & O A Molchanov, Eds, (Terrapub, Tokyo), 2002, pp 173-176.
  - 24 Tronin, A, Thermal IR satellite sensor data application for earth-quake research in China, *Int J Remote Sens (UK)*, 16 (2000) pp 3169-3177.